

Nonlinear focusing of terahertz laser beam by layered superconductor

H.V. Ovcharenko,¹ Z.A. Maizelis,^{1,2} S.S. Apostolov,^{1,2} and V.A. Yampol'skii^{1,2}

¹*V.N. Karazin Kharkov National University, 61077 Kharkov, Ukraine*

²*A.Ya. Usikov Institute for Radiophysics and Electronics NASU, 61085 Kharkov, Ukraine*

We theoretically study the propagation of a terahertz (THz) Gaussian beam through a thin sample of layered superconductor. We consider the beam axis and the layers to be perpendicular to the sample interface, while the electric field in the beam is perpendicular to the layers. In such a geometry, the Josephson current between the superconducting layers supports lensing of the beam instead of divergence on the Rayleigh range. Moreover, due to the nonlinearity, the focal length and transmitted beam waist depend on the incident beam intensity. These dependences show a nontrivial hysteresis behavior that can be observed in experiments with THz lasers.

PACS numbers: 05.45.Ac, 02.50.Ng, 02.60.Lj, 02.30.Hq

I. INTRODUCTION

Over the last years, the physical properties of layered superconductors have attracted the attention of many research groups (see review paper [1] and references therein). The strongly anisotropic high-temperature $\text{Bi}_2\text{Sr}_2\text{CaCu}_2\text{O}_{8+\delta}$, $\text{La}_{2-\delta}\text{Sr}_\delta\text{CuO}_4$, or $\text{La}_{2-\delta}\text{Ba}_\delta\text{CuO}_4$ single crystals are the most prominent examples of these structures [2–5]. Numerous experiments on the c -axis transport in layered high- T_c superconductors justify the use of a model in which the superconducting CuO_2 layers are coupled through the insulator layers by the intrinsic Josephson effect [1, 6, 7]. This makes the layered superconductors to be anisotropic media not only quantitatively, but also qualitatively. While the currents in the plane of layers are of the same nature as in the bulk superconductors, the currents across the layers are caused by the tunneling of quasi-particles.

The Josephson current flowing along the c -axis is coupled with the electromagnetic field inside the insulating layers, thereby providing a specific kind of elementary excitations called Josephson plasma waves (see, e.g., [7, 8]). These waves are of considerable interest because of their THz and sub-THz frequency ranges, which are still hardly reachable for both electronic and optical devices. The frequencies of terahertz waves are in the region of resonance frequencies of molecules and are expected to have many applications [9, 10].

Theoretical studies predict variety of interesting nonlinear phenomena in layered superconductors even in the regime where the Josephson vortices are not formed [6]. This becomes possible for the frequencies not far from the Josephson plasma frequency due to a specific nonlinearity of equations describing the electrodynamics in layered superconductors. In particular, the nonlinearity results in hysteresis response of the system [11–14] and in sensitivity of the system to the external dc-magnetic field [15, 16]. In all these theoretical studies, the irradiation of the sample was considered either by the *plane waves* or in the *waveguide geometry*.

Meanwhile, for experimental investigations of layered superconductor properties, the ZnTe lasers are com-

monly used [1, 17] with the *spatially localized radiation*. These lasers emit femtosecond unit pulses in near-infrared range. Energy, produced by unit pulse, reaches nanojoules with electric field of less than kilovolt per centimeter [18]. As was shown in [11, 19], such fields are well described by linear equations inside layered superconductor. To investigate nonlinear effects, the stronger fields are needed, and to achieve them the main three types of beam generation can be used: the tilted pulse front method [20], the free electron lasers [21], and the gaseous lasers [22].

Tilted pulse method [20, 23, 24] is based on passing of external near-infrared radiation through the nonlinear LiNbO_3 crystal. Due to nonlinear optical effects, frequency of passed radiation is shifted to THz range, which is lower than frequency of incident light. The pulses from such lasers are strongly localized in frequency (1-2%), their duration varies from one to hundreds picosecond, time between pulses is from $5 \cdot 10^{-5}$ s to 10^{-3} s [20, 25], depending on external laser properties. Area of beam cross-section also depends on external laser and varies from 4 mm^2 to 30 cm^2 . The tilted pulse method was used in [26] to investigate response of layered superconductor $\text{La}_{1.84}\text{Sr}_{0.16}\text{CuO}_4$ to terahertz external radiation, as well as to measure frequency dependence of reflectivity and conductivity. To achieve strong electric fields, laser was focused down to 1 mm^2 beam cross-section, thus field increased up to 100 kV/cm . In [26], the frequency of the radiation was 450 GHz , which is below Josephson frequency of 2 THz .

The free electron laser sources use radiation of relativistic electrons, moving in non-homogeneous periodically changing magnetic field [21]. This radiation is also localized in frequency (2 %), however, duration of pulse is tens of picoseconds, and time between pulses is of the order of 10^{-7} s [19, 27, 28]. 2 THz free electron laser with pulse duration of 25 ps was used in Ref. [19] for excitation of the nonlinear Josephson plasma solitons, predicted in Ref. [29] for frequencies close enough to the Josephson plasma frequency. The laser beam was focused to 1 mm^2 beam cross-section, producing 10 kV/cm field.

Recently, rapid development of CO-based gaseous lasers with THz frequencies shows perspective abilities

to use them in investigation of layered superconductors [22, 30, 31]. These lasers produce constant in time radiation with the electric field up to fractions of kilovolts per centimeter. They can be tuned to the pulse regime with the corresponding gain in intensity.

Thus, the high amplitudes sufficient to observe nonlinear effects can be reached by the pulsed radiation. On the other hand, the pulse duration should be long enough in order to establish the stationary field distribution in the sample of layered superconductor. As one can see, the pulse length reachable in experiment is of the order of several centimeters for ~ 100 ps pulses. In the present study we consider samples of several millimeter thickness for which the existing experimental setups can be used to observe the strongly nonlinear effects even taking into account the multiple reflections from the interfaces of the superconducting slab.

In this paper, we theoretically investigate the Gaussian beam which falls on the thin slab of layered superconductor. We consider the case of constant in time beam amplitude, which corresponds to the long enough pulses in experiments. Though the width of the beam does not change significantly in the slab, the curvature of the wavefront becomes negative due to the nonlinearity, resulting in the convergence of the beam. To characterize such nonlinear focusing effect, we introduce focal length F (length from right sample interface to the point, at which width of beam becomes minimal). We find dependences of these parameters on incident beam amplitude and frequency. Also we show that, for the specially chosen frequency and amplitude of the incident beam, the focusing effect may be strongly increased, and the focal length may be significantly decreased down to the distance of nearly 10 cm. Thus, this focusing effect becomes available for the precise experimental investigation.

The paper is organized as follows. In Section II, we describe the model of the beam in vacuum and in layered superconductor and present the main equations for the electromagnetic field in the system. In Section III, taking into account boundary conditions at both interfaces of the slab, we find the curvature of the wave front of the transmitted beam which determines the focal length and the beam waist. In Section IV, we describe the numerical scheme which we use to verify analytic results. Finally, in Section V, we analyze the dependences of focusing characteristics on frequency and amplitude of the incident beam.

II. MODEL

A. Gaussian beam in vacuum

We start our analysis from considering the behavior of the THz Gaussian beam in the vacuum. For the beam propagating along the x -axis, the well-known distribution

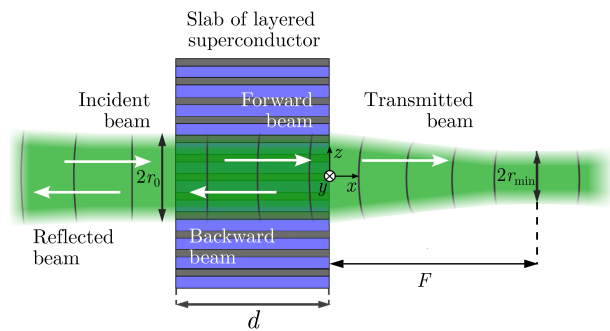


FIG. 1. (Colour online) Schematics of the setup. The laser beam propagates from left to right. The incident beam waist is r_0 at the left interface. The transmitted beam waist is r_{\min} , it is located at the focal length F from the right interface. The x axis is directed along the beam, the z axis is perpendicular to the layers of the superconducting slab of the thickness d . The incident, reflected, and transmitted beams propagate in the vacuum regions, while forward and backward beams propagate inside the superconducting slab (arrows show the beam directions).

of the electric field reads [32, 33],

$$E(x, r, t) = E_0 \exp\left(-\frac{r^2}{r_b^2}\right) \sin\left[k_v\left(x + \frac{\alpha r^2}{2}\right) - \omega t + \phi\right]. \quad (1)$$

Here $r = \sqrt{y^2 + z^2}$ is the distance from the axis of the beam, k_v and ω are the wave-number and frequency, related to each other by the dispersion relation $k_v = \omega/c$, c the speed of light. The amplitude E_0 , characteristic radius r_b , wave-front curvature α , and the Gouy phase ϕ are the main characteristics of the beam. Being governed by the Maxwell equations, they vary along the beam path, thus being the functions of x .

Consider the propagation of the beam with initial radius $r_b(x=0) = r_0$ and initial negative wavefront curvature $\alpha(x=0) = -\alpha_0 < 0$ (see Fig. 1). The beam radius $r_b(x)$ obeys the following relation [32]:

$$r_b(x) = r_{\min} \left[1 + \frac{4(x-F)^2}{k_v^2 r_{\min}^4}\right]^{1/2}, \quad (2)$$

demonstrating convergence of the beam to the minimal reachable radius r_{\min} called the beam waist,

$$r_{\min} = r_0 \left[1 + \frac{\alpha_0^2 k_v^2 r_0^4}{4}\right]^{-1/2}, \quad (3)$$

at a distance F from the initial point, that we call the focal length,

$$F = -\frac{1}{\alpha_0} \left[1 + \frac{4}{\alpha_0^2 k_v^2 r_0^4}\right]^{-1}. \quad (4)$$

In the present paper, we investigate the beam that transmits through the slab of layered superconductor. To

be specific, we suppose that the waist point of incident beam coincides with the slab interface, thus the beam curvature in this point is zero. In common media, after such point, the beam should diverge on the Rayleigh range. However, we show that even thin slab of layered superconductor can make the curvature of the beam negative, thus producing the focusing effect (although it does not change practically the radius of the beam within the slab).

B. Gaussian beam in a slab of layered superconductor

We focus our attention on the case when laser beam falls perpendicularly on a surface of a layered superconductor sample, which leads to the strong focusing of the beam without its distortion. We are aiming to study the situation when the Josephson tunneling current across the layer is excited. The simplest geometry for that is when *the layers are perpendicular to the slab interface*, which we consider here, see Fig. 1. Note, that the opposite simple geometry, when the layers of the slab are parallel to the interface, is not interesting for our study, because the electric field of the beam lays in the plane of superconducting layers, and the medium behaves like the bulk superconductor with linear electrodynamics.

The slab interface in the considered setup is anisotropic, which makes the system highly sensitive to the polarization of the radiation. Actually, the layered superconductor slab acts as a THz polarization filter in a wide frequency range. Indeed, if the electric field in the incident wave is directed along the layers of the slab, we again face the situation with superconducting currents flowing only along the layers, and the so-called ordinary waves are excited in the sample. These ordinary waves, as was shown in [1], for characteristic frequencies not far from Josephson frequency ω_J , evanesce inside the sample on the characteristic depth of $\lambda_{ab} \sim 10^{-5}$ cm, which makes the sample totally reflective for the realistic experimental situations. On the contrary, the linear polarization for which the electric field is directed perpendicularly to the layers, generates Josephson current and excites the so-called extraordinary waves in the slab, which are nonlinear. Here we focus on the certain polarization with *the electric field perpendicular to the layers*, which induces only extraordinary waves and results in the nonlinear focusing of transmitted beam.

It is important to take into account the reflections on each of the sample interfaces. Thus, we take into account incident, reflected and transmitted beams in vacuum regions and the beams, propagating in both directions in the superconducting slab. It should be noted that, in general, the electromagnetic field inside the slab could not be represented as the only two, forward and backward, Gaussian beams. Firstly, the Gaussian profile could be lost due to superposition of numerous reflected beams and, secondly, all these reflections could pump energy

into each other due to nonlinearity of the system. However, we study the thin slabs, and this assumption allows us overcome the mentioned problems.

Namely, we assume here that the thickness of the slab is of order of effective wavelength inside the slab and that the radius of the beam is much greater than the characteristic penetration length along the layers $\lambda_c = c/(\omega_J\sqrt{\varepsilon})$, where ε is the permittivity of the insulating layers in the slab. These assumptions are fulfilled for the realistic experimental implications of the THz beams (see, for example, [19]), and allow one to consider the radius and, thus, amplitude of each reflected beam inside the slab to be constants. Indeed, using for the estimation Eq. (2) with the wavenumber k_s of linear waves in superconductor [1, 6],

$$k_s^2 = \varepsilon(\omega^2 - \omega_J^2)/c^2, \quad (5)$$

and characteristic parameters $\omega_J/2\pi = 2$ THz, $\omega - \omega_J = 10^{-3}\omega_J$, we get $\Delta r/r \sim 10^{-4}$, where Δr is the variation of the thickness in the slab. Also this estimation is verified by numerical simulation, see for the details Section IV. Therefore, superposition of all the forward (backward) beams of the same radius can be regarded as a single forward (backward) beam.

So, taking into account the numerous reflections from the slab interfaces, in the assumption of small sample thickness and nearly unchanged beam width, we can seek the electric field in the slab in the form of two Gaussian beams of the same radius r_0 , propagating in forward (index “+”) and backward (index “-”) directions,

$$E_s(x, r, t) = \mathcal{E}_0 \exp\left(-\frac{r^2}{r_0^2}\right) \left(E_+ \sin \Phi_+ + E_- \sin \Phi_-\right), \quad (6)$$

where the total phases Φ_+ and Φ_- are

$$\Phi_{\pm} = \pm k_{\pm}(r) \left(x + \frac{\alpha_{\pm} r^2}{2}\right) - \omega t + \phi_{\pm}. \quad (7)$$

Here $\mathcal{E}_0 = \Phi_0/2\pi s\lambda_c$ is a characteristic scale of electric and magnetic fields in layered superconductor, $\Phi_0 = \pi\hbar/e$ is magnetic flux quantum, s is the period of the layered superconductor structure. Parameters α_{\pm} and ϕ_{\pm} are considered here to be constants, which is correct for the thin samples. This means that in the linear approximation the curvature of the wave-front would not distinctly change. However, in nonlinear regime we should take into account the radial dependency of the wave number $k_{\pm}(r)$, because intensity of the electromagnetic field depends on the distance r to the axis of the beam. Therefore, the cross-terms depending on both r and x appear in phase that means the effective curvature of the wave-front changes along the propagation of the beam, see Eq. (16) for details. In other words, due to the nonlinearity, different regions of the wave-front have different speeds, and this makes the beam converge after passing the slab. The latter is the mechanism of the nonlinear focusing of the THz radiation by the layered superconductor.

C. Electrodynamics of layered superconductor

To find the nonlinear wave-number $k_{\pm}(r)$ we now briefly describe the electrodynamics of layered superconductor. The field inside the slab is determined by the gradient invariant phase difference φ of order parameter in the neighboring superconducting layers of the slab [6]. This parameter is actually discrete, but here we consider rather thick beams in comparison with the period of the layered superconductor structure, $r_0 \gg s$, and the continual approximation is valid. In the considered geometry the electric field is oriented perpendicular to the layers and induces the Josephson tunneling current, $J_z = J_c \sin \varphi$ with J_c being the maximal value of Josephson current density. Meanwhile, the current along the layers induced by the magnetic field of the beam can be described by the London model, $J_x = -c/(4\pi\lambda_{ab}^2) A_x$, where A_x is the x -component of the vector potential in the slab. In [6] it was shown, that the calibration for the vector potential may be chosen in such way that for the z -component A_z the following relation is valid, $\varphi = -2\pi s A_z / \Phi_0$.

Then, using Maxwell equations and relation of electromagnetic field with vector potential, one can express the electric and magnetic components of the field via the phase difference φ ,

$$E_s = -\mathcal{E}_0 \frac{1}{\omega_J \sqrt{\varepsilon}} \frac{\partial \varphi}{\partial t}, \quad (8)$$

$$\frac{\partial H_s}{\partial x} = -\frac{\mathcal{E}_0}{\lambda_c} \left[\frac{1}{\omega_J^2} \frac{\partial^2 \varphi}{\partial t^2} + \sin \varphi \right], \quad (9)$$

and derive the differential equation [6, 34], which is the continualization of the well-known coupled sin-Gordon equations,

$$\left(1 - \lambda_{ab}^2 \frac{\partial^2}{\partial z^2}\right) \left[\frac{1}{\omega_J^2} \frac{\partial^2 \varphi}{\partial t^2} + \sin \varphi \right] - \lambda_c^2 \left(\frac{\partial^2 \varphi}{\partial x^2} + \frac{\partial^2 \varphi}{\partial y^2} \right) = 0. \quad (10)$$

Here the Josephson plasma frequency ω_J is related to the other parameters of the layered superconductor, $\omega_J = \sqrt{8\pi e s J_c / (\hbar \varepsilon)}$.

It is important to understand that in spite of strong anisotropy of the layered superconductor, the Gaussian beam propagating through the thin slab nearly preserves its axial symmetry of the amplitude distribution in its cross-section. Indeed, the terms with second derivatives over y and z in Eq. (10) appear to be small in comparison to other terms, if the slab is thin, $d \ll r_0$. We additionally verify this assumption comparing the cross-sectional distribution in y and z calculated in numerical simulation with correspondent analytical results, see Section IV and Fig. 2 for details.

The nonlinearity of Eqs. (9) and (10) leads in principal to the generation of higher harmonics both in space and time coordinates. As was reported in [6], this generation can be neglected, when the phase difference φ is small and $\sin \varphi$ may be expanded into series up to the third

order, $\sin \varphi \approx \varphi - \varphi^3/6$. In general, such approximation provides only weak nonlinear effects. However, there is an important range of frequencies, close enough to ω_J , when the nonlinearity plays crucial role [6]. The strong nonlinear effects may be observed when

$$\varphi \sim \beta \equiv \sqrt{\omega^2/\omega_J^2 - 1} \ll 1, \quad (11)$$

because linear terms in Eq. (10) nearly cancel each other and the cubic term may become significant. In the present paper we study this frequency range and predict strong nonlinear focusing of the Gaussian beam.

As for the radial coordinate r , we expand all the dependencies in series over small r/r_0 up to the second order, as we suppose that the Gaussian distribution for thick beams is preserved. We find the phase difference φ from Eq. (8) with the electric field E_s in the form of Eq. (6) and, then, substitute it in Eq. (10). Neglecting higher spatial and temporal harmonics, the nonlinear wave-numbers $k_{\pm}(r)$ can be related with amplitudes E_{\pm} of the forward and backward beams via parameters κ_{\pm} ,

$$k_{\pm}(r) = k_s + \frac{\kappa_{\pm}}{\lambda_c} - \frac{\gamma_{\pm}}{\lambda_c} \frac{r^2}{r_0^2}, \quad (12)$$

$$8\kappa_{\pm}(2\beta + \kappa_{\pm}) = \varepsilon(E_{\pm}^2 + 2E_{\mp}^2), \quad (13)$$

$$\gamma_{\pm} = \kappa_{\pm} \frac{2\beta + \kappa_{\pm}}{\beta + \kappa_{\pm}}, \quad (14)$$

where k_s is the wavenumber of linear waves, Eq. (5). Note, that the wavenumbers for the forward and backward propagating beams are tangled with each other via their amplitudes as it is natural in a nonlinear problem.

The first term of Eq. (12) corresponds to the linear limit of small amplitudes, and the second and the third terms are the effect of nonlinearity. The important effect of nonlinearity is that wave-numbers $k_{\pm}(r)$ depend on radial coordinate, which means, that the curvature of the beam changes along its path. Indeed, recombining terms with r^2/r_0^2 in Eq. (7) and neglecting terms $\propto (r/r_0)^4$, we can express Φ_{\pm} in the following form,

$$\Phi_{\pm} = \pm k_{\pm}^{(0)} \left[x + \frac{\alpha_{\pm}^{\text{eff}}(x) r^2}{2} \right] - \omega t + \phi_{\pm}, \quad (15)$$

introducing the effective curvature $\alpha_{\pm}^{\text{eff}}(x)$,

$$\alpha_{\pm}^{\text{eff}}(x) = \alpha_{\pm} - \frac{2\gamma_{\pm}}{\lambda_c k_{\pm}^{(0)} r_0^2} x, \quad k_{\pm}^{(0)} = k_{\pm}(r=0). \quad (16)$$

Note, that strictly speaking Eqs. (12) and (15) are valid only for $r/r_0 \ll 1$, however, practically work for all r , where $\exp[-(r/r_0)^2] \sim 1$, see Section IV and Fig. 2 for details.

For magnetic field (which is directed along y axis) we derive

$$H_s(x, r, t) = \mathcal{E}_0 \exp\left(-\frac{r^2}{r_0^2}\right) \left(H_+ \sin \Phi_+ + H_- \sin \Phi_- \right), \quad (17)$$

with dimensionless amplitudes H_{\pm} related to E_{\pm} ,

$$H_{\pm} = \mp \sqrt{\varepsilon} E_{\pm} (\beta + \kappa_{\pm}). \quad (18)$$

Now as we have the expressions for the electromagnetic field in the superconducting slab, we proceed with finding the parameters E_{\pm} , α_{\pm} , ϕ_{\pm} in superconductor and amplitudes, curvatures and phases of the reflected and transmitted waves in vacuum.

III. FOCUSING OF THE GAUSSIAN BEAM BY THE LAYERED SUPERCONDUCTOR SLAB

In this section we derive an analytic expression for the curvature α_t in the transmitted beam that defines the focal length F and the waist r_{\min} of the beam. To that purpose we should relate the parameters of the beams in vacuum and the slab of layered superconductor by matching the tangential components of the electromagnetic field at the interfaces. In the slab we use Eqs. (6) and (17), while in the vacuum regions the corresponding expressions can be written analogously to Eq. (1). Aiming to determine the curvatures and phases of the incident, reflected and transmitted beams at the interfaces, we present the field only in the vicinity of the slab. There we can set the radius of all beams to r_0 as well as in the slab. Then, in the left vacuum region (see Fig. 1) there are the incident and reflected beams,

$$E_L(x, r, t) = \exp\left(-\frac{r^2}{r_0^2}\right) (E_i \sin \Phi_i + E_r \sin \Phi_r), \quad (19)$$

and in the right vacuum region there is the transmitted beam only,

$$E_R(x, r, t) = E_t \exp\left(-\frac{r^2}{r_0^2}\right) \sin \Phi_t. \quad (20)$$

Here the phases of transmitted Φ_t and reflected Φ_r beams are defined as follows,

$$\Phi_{t,r} = \pm k_v \left(x + \frac{\alpha_{t,r} r^2}{2}\right) - \omega t + \phi_{t,r}, \quad (21)$$

with signs $+$ and $-$ corresponding to indices t and r , respectively. Curvatures α_r and α_t as well as Gouy phases ϕ_r and ϕ_t can be considered as constants only in the vicinity of the slab and are to be determined from the boundary conditions. Once they are found, it can be considered as initial values for the correspondent beams to determine the focal length and the beam waist.

The total phase Φ_i of the incident beam we choose in the following simple form,

$$\Phi_i = k_v x - \omega t, \quad (22)$$

which means that the incident beam waist position, where the curvature is absent, $\alpha_i = 0$, coincides with the left interface.

The corresponding magnetic field in the vacuum can be easily obtained from Maxwell's equations,

$$\begin{aligned} H_L(x, r, t) &= \exp\left(-\frac{r^2}{r_0^2}\right) (-E_i \sin \Phi_i + E_r \sin \Phi_r), \\ H_R(x, r, t) &= -E_t \exp\left(-\frac{r^2}{r_0^2}\right) \sin \Phi_t. \end{aligned} \quad (23)$$

Now we can match the tangential components of the electric and magnetic fields on the two interfaces between vacuum and the slab. To get the close set of equation for the sought quantities, we expand the fields as the functions of r into series and keep the summands up to the second order in r/r_0 only. Straightforward calculations yield the following equations, determining the amplitudes E_{\pm} of the two beams in the slab,

$$\begin{aligned} E_+ + E_- + H_+ + H_- &= 0, \\ \frac{E_+ - E_-}{2} \sin\left[k_s d + \frac{d}{2\lambda_c} (\kappa_+ + \kappa_-)\right] &= \frac{E_i}{\mathcal{E}_0}. \end{aligned} \quad (24)$$

Recall here that H_{\pm} are related to E_{\pm} by Eq. (17), and κ_{\pm} are determined by Eq. (13). Therefore, the values of E_{\pm} appear to be nonlinear functions of the amplitude E_i of the incident beam. Moreover, these dependencies may be multi-valued, which we will discuss further in Section V.

Another result of matching the fields on the vacuum-slab interfaces is the expression for the curvature of the wave-front of the transmitted beam, which is valid for the amplitudes E_{\pm} small enough as compared to β (and yet these amplitude may be high enough for the nonlinear effects to be pronounced),

$$\alpha_t = \frac{2d}{k_v r_0^2} \frac{\gamma_+ E_+ - \gamma_- E_-}{E_+ + E_-}. \quad (25)$$

It can be shown, that this curvature is negative and thus the beam converges. One can substitute this value to Eqs. (3) and (4), $\alpha_0 = \alpha_t$, and thus find the waist r_{\min} of the transmitted beam and the focal length F , which determine the focusing ability of the superconducting slab.

IV. NUMERICAL SIMULATION

Before analyzing the waist of the transmitted beam and the focal length as functions of system parameters, we describe our numerical simulation scheme, worked out to verify the obtained analytic results. It should be emphasized that in our analytic approach we make several important assumptions, such as neglecting of higher spatial and temporal harmonics, and invariance of the radius and the Gaussian profile of the beam inside the slab. In order to check them to be correct we perform a direct numerical simulation of Eq. (10) for the phase difference φ as a function of coordinates x, y, z and time t inside the slab of layered superconductor, while the incident, reflected, and transmitted beams are accounted by the

corresponding boundary conditions for electric and magnetic fields at each point of the slab interfaces. Additionally, we take into account the conditions of free radiation for the reflected and transmitted beams, which is standard routine in numerical simulations of spatially unbounded systems.

The size of the sample is considered to be in $N = 3$ times greater than the diameter of the beam, namely $2.1 \text{ cm} \times 2.1 \text{ cm}$ for the 7 mm wide laser. These dimensions are high enough to neglect the edge effects due to the fact that the electromagnetic field is in $\exp(N^2)$ times weaker at the lateral edges than on the axis of the beam.

Technically, the numerical simulation of Eq. (10) is performed for several values of the incident beam amplitude. For each value E_i the following procedure is performed. The amplitude is gradually increased from zero to E_i slowly enough and then kept constant, until the electromagnetic field in the whole sample becomes well established. The obtained distribution of the field is used to estimate deviations from the expected analytic result and to calculate the focusing parameters of the transmitted beam.

Figure 2 shows the total phase

$$\Delta\Phi_t(y, z) = \Phi_t(y, z, t) - \Phi_t(y = 0, z = 0, t)$$

with respect to the central point of the cross-section (panels *a* and *c*) and the amplitude (panels *b* and *d*) of electric field, i.e. the maximal value of electric field in each point (y, z) , in the transmitted beam at the right interface, $x = 0$. The panels *a* and *b* present the distribution of these quantities as functions of spatial coordinates y and z by color gradient obtained by the numerical simulation. The panels *c* and *d* are assigned for accurate comparison of these numerical distributions with analytic results. Namely, the green curves present the total phase $\Delta\Phi_t(r) = \Phi_t(r, t) - \Phi_t(r = 0, t)$ (panel *c*) and the amplitude $E_t \exp(-r^2/r_0^2)$ (panel *d*) as function of the spatial coordinate r , calculated by analytic approach described in Section III. The blue and red lines with solid circles and empty squares correspond to the numerical distributions in two perpendicular cross-sections, vertical (at $y = 0$ as function of z) and horizontal (at $z = 0$ as function of y), respectively. The same colors are used for the dashed straight lines in panels *a* and *b* to indicate corresponding cross-sections.

As can be seen from panels *c* and *d* of Fig. 2, even for the intensive enough incident beam with amplitude $E_i = 4 \text{ kV/cm}$, where nonlinear effects are distinctly pronounced (see Section V and Fig. 4 for details), the field distribution appears to be nearly isotropic and Gaussian. Note that the seeming deviation of the amplitude from the Gaussian in the region of small radii is due to a slightly narrower distribution of the beam in the simulation, which results in the higher amplitude in the central part. The total phase is well consistent with the quadratic dependence as assumed in the model, while the deviation far from the beam axis are inessential

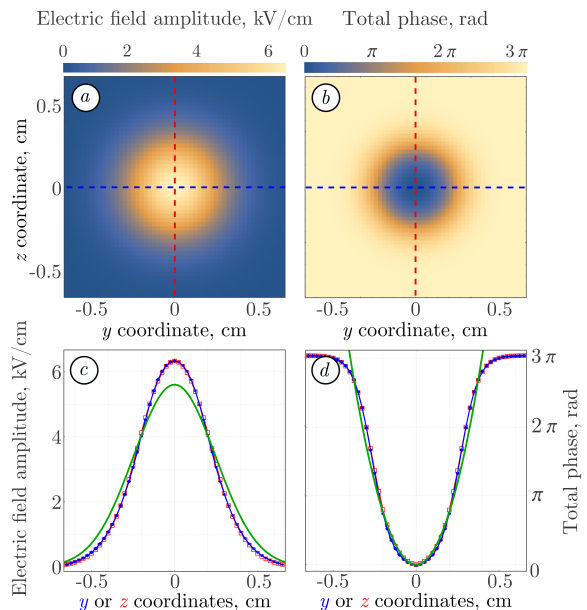


FIG. 2. (Color online) Spatial distributions of the amplitude (panels *a* and *c*) and the total phase (panels *b* and *d*) of electric field in the transmitted beam at the right interface. Panels *a* and *b* show the distributions obtained by the numerical simulation as functions of spatial coordinates y and z by the color gradient. Panels *c* and *d* presents these numerical distributions in two perpendicular cross-sections, vertical (at $y = 0$ as function of z) and horizontal (at $z = 0$ as function of y), plotted by the blue lines with solid circles and red lines with empty squares in comparison with the analytic distributions (as function of r), plotted by the green lines and calculated as described in Section III. The same blue and red colors are used for the dashed straight lines in panels *a* and *c* to indicate respective cross-sections. The distributions are calculated for the incident beam amplitude $E_i = 9 \text{ kV/cm}$ with pronounced nonlinear effects. Other parameters are: $\omega_J/2\pi = 2 \text{ THz}$, $\lambda_c/\lambda_{ab} = 15$, $r_0 = 3.5 \text{ mm}$, $d = 2.5 \text{ mm}$, $s = 2 \cdot 10^{-7} \text{ m}$, $\varepsilon = 15$.

there because of the exponentially small amplitude, i.e. $\exp[-(r/r_0)^2] \ll 1$.

So, the numerical simulation ensures that our assumptions made in the model are reasonable and we can use analytic results to study the nonlinear focusing of the Gaussian beam by layered superconductor.

V. ANALYSIS OF THE RESULTS

In this section we apply both the analytic approach and numerical simulation to study the dependence of focal length and the waist of the transmitted beam on the frequency and amplitude of the incident radiation.

We start from the dependence on frequency, which is especially interesting in the vicinity of the Josephson plasma frequency ω_J . Figure 3 shows the dependence of the focal length F (lower blue curve) and the waist

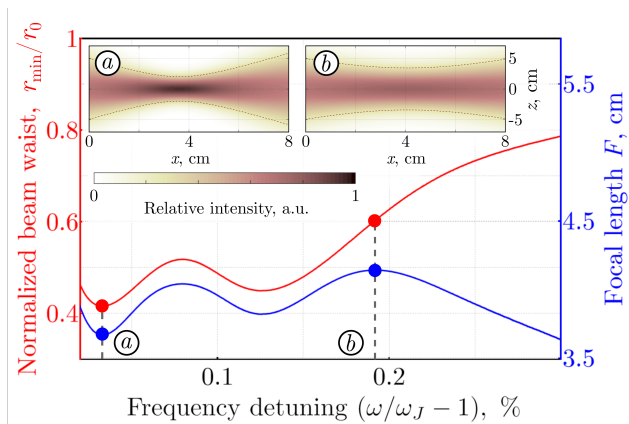


FIG. 3. (Colour online) Dependence of focal length F (lower blue curve) and normalized beam waist r_{\min}/r_0 (upper red curve) on frequency detuning of the incident beam. Points a and b correspond to the local minimum at $\omega/\omega_J - 1 \approx 0.3 \cdot 10^{-3}$ and maximum at $\omega/\omega_J - 1 \approx 1.9 \cdot 10^{-3}$ on the lower curve. The amplitude of incident beam $E_i = 9$ kV/cm. The insets show the intensity distribution in the transmitted beam for frequencies of points a and b , while dashed curves show $1/e^2$ width. Other parameters are the same as in Fig. 2.

r_{\min}/r_0 of the transmitted beam normalized by the initial radius (upper red curve) as the functions of frequency detuning $\omega/\omega_J - 1$ counted in percents. We can see, that as the frequency ω of laser beam approaches ω_J , both the focal length and beam waist start to pronouncedly oscillate. Physically these oscillations emerge from the variation of the wavelength in the sample, and are analogous to the Fabry–Pérot oscillations. Indeed, the critical points of the curves in Fig. 3 correspond to the frequencies, for which the thickness of the sample is integer number of wavelengths, $2\pi n/k_{\pm}^{(0)}$. However, the wavelength appears not proportional to ω as in linear optics, but nonlinearly depends on frequency detuning $\omega/\omega_J - 1$, significantly affecting not only the amplitude of the transmitted beam, but also the focal length and the beam waist. It should be noted, that for plain waves and wave-guide modes, see Refs. [12, 13], the same oscillations with frequency detuning $\omega/\omega_J - 1$ was predicted for the transmission coefficient (the ratio of amplitudes of transmitted and incident wave), which sharply increases near the critical points reaching nearly full transmittance. So, the nonlinear effects lead not only to rapid increase of amplitude, but also to strong focusing effect of the Gaussian beam.

Now let us analyze the effect of the beam intensity, which also comes from the nonlinearity of the problem. Figure 4 shows the dependence of the focal length (upper panel) and transmitted beam waist (lower panel) on the amplitude of the incident beam. It is important, that according to Eq. (16) with κ_{\pm} from Eq. (13), the dependence of the curvature α_t on the incident beam amplitude E_i is implicit and strongly nonlinear. Subsequently, the transmitted beam parameters appear not only non-monotonic as functions of E_i , but even multi-

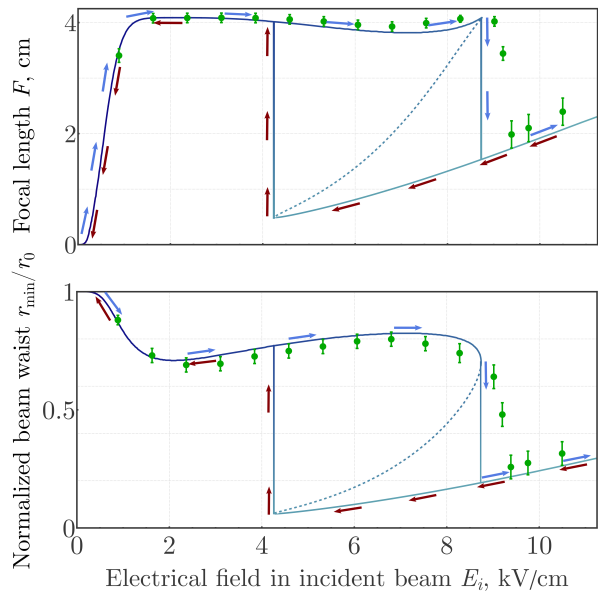


FIG. 4. (Colour online) Dependencies of transmitted beam waist (lower panel) and focal length (upper panel) on amplitude of the incident beam. Solid and dotted curves show reachable and unreachable branches. Arrows show possible hysteresis variation of the focusing parameters, when the incident beam intensity increases/decreases gradually. Green points show the results of the numerical simulation. Frequency detuning is $\omega/\omega_J - 1 = 1.1 \cdot 10^{-3}$, the rest of parameters are the same as for Fig. 3.

valued [12, 13] as seen from Fig. 4.

One can see from Fig. 4 that each of dependencies $F(E_i)$ and $r_{\min}(E_i)$ involves three branches. The first branch starts at $E_i = 0$ and ends up at a certain critical value $E_{i,1}$, while the third branch starts at a certain critical value $E_{i,2}$ and goes to the greater values. The second middle branch (marked by dotted line), placed between $E_{i,2}$ and $E_{i,1}$, is unreachable as usual for such multi-valued dependencies.

If one gradually increases/decreases the amplitude of the incident beam, the parameters of the transmitted beam may exhibit hysteresis behavior, marked in Fig. 4 by arrows. Specifically, if amplitude E_i of incident beam is increased up to $E_{i,1}$ ($E_{i,1} \approx 8.8$ kV/cm for a chosen parameters), the focal length and the transmitted beam waist gradually change along the first upper branch. But if amplitude goes over this critical value, the jump to another branch is unavoidable. Further increase of amplitude leads to a slight weakening of focusing effect along the third lower branch. As we then decrease amplitude, the variation of the focusing parameters follows the third lower branch of the curve, and the jump now occurs for the amplitude $E_{i,2}$ ($E_{i,2} \approx 4.2$ kV/cm for the chosen parameters).

The green points with vertical error bars in Fig. 4 show the results of the numerical simulation described in Section IV. Errors are estimated by the numerical accuracy

of the simulation. One can see that the simulation points fit well the analytic curve, and the deviation can be noticed only in the vicinity of $E_{i,1}$, when jump between the first and third branches occurs. It should be noted that the simulation shows single-valued dependencies $F(E_i)$ and $r_{\min}(E_i)$, confirming the first branch and the part of the third branch (for $E_i > E_{i,1}$ only). We try several strategies to achieve the other part of the third branch in the simulation (for $E_{i,2} < E_i < E_{i,1}$), but the numerical scheme converges to the values of the first branch. So, it is an open problem to find out whether correspondent values of the third branch can be attained in the numerical simulation or in the real experiment. Yet, we clearly see that our analytic approach well fits the results of numerical simulation and, thus, can be used to predict the behavior of laser beam in nonlinear layered superconducting slabs and describe its focusing parameters.

VI. CONCLUSIONS

In this paper we have studied theoretically propagation of the Gaussian laser beam through the layered superconductor slab with layers perpendicular to the slab interface. We have chosen polarization where the electric field is perpendicular to the layers thus inducing Josephson currents in the sample. Solving differential equations for the electromagnetic field distribution in the slab with ap-

propriate boundary conditions, accounting for the reflections on the interfaces, we have presented the dependencies of the focal length and the transmitted beam waist on the frequency and amplitude of the incident beam in an implicit, but algebraic form. Also we have conducted the numerical simulation to determine the field distribution in the slab and, thus, verified the analytic results.

We have shown that in nonlinear regime laser beam, after passing the layered superconductor slab, acquires the negative curvature of the wavefront, which leads to the focusing of the beam. The focusing effect strongly depends on both amplitude and frequency of the incident radiation, and becomes more pronounced for the frequencies, which are closer to Josephson plasma frequency, and for high enough amplitudes. Moreover, the analysis of the results admits that the focal length and the transmitted beam waist may show hysteresis behavior, when the amplitude is increased and then decreased gradually.

VII. ACKNOWLEDGMENT

We gratefully acknowledge support from the National Research Foundation of Ukraine, Project No. 2020.02/0149 “Quantum phenomena in the interaction of electromagnetic waves with solid-state nanostructures”.

-
- [1] Y. Laplace and A. Cavalleri, *Advances in Physics: X* **1**, 387 (2016).
 - [2] P. J. Curran, H. A. Mohammed, S. J. Bending, A. E. Koshelev, Y. Tsuchiya, and T. Tamegai, *Scientific Reports* **8**, 10914 (2018).
 - [3] D. Nicoletti, D. Fu, O. Mehio, S. Moore, A. S. Disa, G. D. Gu, and A. Cavalleri, *Phys. Rev. Lett.* **121**, 267003 (2018).
 - [4] M. Hücker, M. v. Zimmermann, Z. J. Xu, J. S. Wen, G. D. Gu, and J. M. Tranquada, *Phys. Rev. B* **87**, 014501 (2013).
 - [5] V. Khanna, R. Mankowsky, M. Petrich, H. Bromberger, S. A. Cavill, E. Möhr-Vorobeva, D. Nicoletti, Y. Laplace, G. D. Gu, J. P. Hill, M. Först, A. Cavalleri, and S. S. Dhesi, *Phys. Rev. B* **93**, 224522 (2016).
 - [6] S. Savel'ev, V. A. Yampol'skii, A. L. Rakhmanov, and F. Nori, *Rep. Prog. Phys.* **73**, 026501 (2010).
 - [7] X. Hu and S.-Z. Lin, *Superconductor Science and Technology* **23**, 053001 (2010).
 - [8] Y. O. Averkov, V. M. Yakovenko, V. A. Yampol'skii, and F. Nori, *Phys. Rev. B* **87**, 054505 (2013).
 - [9] P. Salén, M. Basini, S. Bonetti, J. Hebling, M. Krasilnikov, A. Y. Nikitin, G. Shamuilov, Z. Tibai, V. Zhaunerchyk, and V. Goryashko, *Physics Reports* **836-837**, 1 (2019).
 - [10] I. E. Batov, X. Y. Jin, S. V. Shitov, Y. Koval, P. Müller, and A. V. Ustinov, *Applied Physics Letters* **88**, 262504 (2006).
 - [11] V. A. Yampol'skii, T. M. Slipchenko, Z. A. Mayzelis, D. V. Kadygrob, S. S. Apostolov, S. E. Savel'ev, and F. Nori, *Phys. Rev. B* **78**, 184504 (2008).
 - [12] S. S. Apostolov, Z. A. Maizelis, M. A. Sorokina, V. A. Yampol'skii, and F. Nori, *Phys. Rev. B* **82**, 144521 (2010).
 - [13] T. N. Rokhmanova, S. S. Apostolov, Z. A. Maizelis, V. A. Yampol'skii, and F. Nori, *Phys. Rev. B* **88**, 014506 (2013).
 - [14] T. N. Rokhmanova, S. S. Apostolov, Z. A. Maizelis, V. A. Yampol'skii, and F. Nori, *Phys. Rev. B* **90**, 184503 (2014).
 - [15] S. S. Apostolov, Z. A. Maizelis, N. M. Makarov, F. Pérez-Rodríguez, T. N. Rokhmanova, and V. A. Yampol'skii, *Phys. Rev. B* **94**, 024513 (2016).
 - [16] N. Kvitka, S. S. Apostolov, N. M. Makarov, T. Rokhmanova, A. A. Shmat'ko, and V. A. Yampol'skii, *Phys. Rev. B* **103**, 104512 (2021).
 - [17] H.-T. Lee, G.-S. Ji, J.-Y. Oh, C.-W. Seo, B.-W. Kang, K.-W. Kim, and H.-R. Park, **11**, 651 (2021).
 - [18] S. Vidal, J. Degert, M. Tondusson, E. Freysz, and J. Oberlé, *Journal of the Optical Society of America B* **31**, 149 (2013).
 - [19] A. Dienst, E. Casandruc, D. Fausti, L. Zhang, M. Eckstein, M. Hoffmann, V. Khanna, N. Dean, M. Gensch, S. Winnerl, W. Seidel, S. Pyon, T. Takayama, H. Takagi, and A. Cavalleri, *Nature materials* **12** (2013).
 - [20] L. Wang, G. Tóth, J. Hebling, and F. Kärtner, *Laser & Photonics Reviews* **14**, 2000021 (2020).

- [21] Z. Huang and K.-J. Kim, Phys. Rev. ST Accel. Beams **10**, 034801 (2007).
- [22] P. Chevalier, A. Amirzhan, F. Wang, M. Piccardo, S. G. Johnson, F. Capasso, and H. O. Everitt, Science **366**, 856 (2019).
- [23] P. S. Nugraha, G. Krizsán, C. Lombosi, L. Pálfalvi, G. Tóth, G. Almási, J. A. Fülöp, and J. Hebling, Optics Letters **44**, 1023 (2019).
- [24] J. Hebling, K. L. Yeh, M. C. Hoffmann, B. Bartal, and K. A. Nelson, Journal of The Optical Society of America B-optical Physics **25** (2008).
- [25] Y. Avetisyan, A. Makaryan, V. Tadevosyan, and M. Tonouchi, Journal of Infrared, Millimeter, and Terahertz Waves **38**, 1439 (2017).
- [26] A. Dienst, M. C. Hoffmann, D. Fausti, J. C. Petersen, S. Pyon, T. Takayama, H. Takagi, and A. Cavalleri, Nature Photonics **5**, 485 (2011).
- [27] N. Piovella and L. Volpe, Atoms **9**, 28 (2021).
- [28] R. Huang, W. Li, Z. Zhao, H. Li, J. Wang, T. Ma, Q. Huang, Z. He, Q. Jia, L. Wang, and Y. Lu, Particles **1**, 267 (2018).
- [29] R. Rajaraman, *Solitons and Instantons: An Introduction to Solitons and Instantons in Quantum Field Theory* (Elsevier Science Ltd, 1982).
- [30] L. Bosco, M. Franckić, G. Scalari, M. Beck, A. Wacker, and J. Faist, Applied Physics Letters **115**, 010601 (2019).
- [31] F. Wang, J. Lee, D. J. Phillips, S. G. Holliday, S.-L. Chua, J. Bravo-Abad, J. D. Joannopoulos, M. Soljačić, S. G. Johnson, and H. O. Everitt, Proceedings of the National Academy of Sciences **115**, 6614 (2018).
- [32] D. S. Simon, *A Guided Tour of Light Beams: From lasers to optical knots* (IOP Publishing, 2016).
- [33] R. Guenther, *Modern Optics*, Wiley international edition (Wiley, 1990).
- [34] S. N. Artemenko and S. V. Remizov, Journal of Experimental and Theoretical Physics Letters **66**, 853 (1997).